




Optimized control for high-fidelity state transmission in open systemsYang-Yang Xie ¹, Feng-Hua Ren,² Arapat Ablimit,¹ Xiang-Han Liang,¹ and Zhao-Ming Wang ^{1,*}¹*College of Physics and Optoelectronic Engineering, Ocean University of China, Qingdao 266100, People's Republic of China*²*School of Information and Control Engineering, Qingdao University of Technology, Qingdao 266520, People's Republic of China* (Received 1 May 2023; revised 2 August 2023; accepted 17 August 2023; published 1 September 2023)

Quantum state transfer through spin chains has been extensively investigated. Two schemes, the coupling set for perfect state transfer (PST) or adding a leakage elimination operator (LEO) Hamiltonian have been proposed to boost the transmission fidelity. However, these ideal schemes are only suitable for closed systems and will lose their effectiveness in open ones. In this work, we invoke a well-explored optimization algorithm, Adam, to expand the applicable range of PST couplings and LEO to the open systems. Our results show that, although the transmission fidelity decreases with increasing system-bath coupling strength, Markovianity and temperature for both ideal and optimized cases, the fidelities obtained by the optimized schemes always outweigh the ideal cases. The enhancement becomes bigger for a stronger bath, indicating a stronger bath provides more space for the Adam to optimize. This method will be useful for the realization of high-fidelity information transfer in the presence of environment.

DOI: [10.1103/PhysRevA.108.032401](https://doi.org/10.1103/PhysRevA.108.032401)**I. INTRODUCTION**

High-fidelity information transfer between qubits lays a firm foundation for the realization of large-scale fault-tolerant quantum computers [1,2]. Spin qubits interact through nearest-neighbor Heisenberg exchange coupling and constitute a one-dimensional spin chain. Bose proposed to use a spin chain as the channel for short-distance communication [3]. Nonetheless, the transmission fidelity decreases with the increasing number of spins [3,4]. Many strategies for the fidelity improvement have been proposed, such as arranging the special couplings between nearest-neighbor sites for perfect state transfer (PST) [5,6], adding well-designed external fields [7–10]. Quantum state transfer (QST) has also been experimentally investigated in a variety of platforms, including superconducting qubit chains [11], trapped ions [12], ultracold atoms [13], semiconductor quantum dots [14,15], and so on.

Along with the above alluded to ones, the proposed schemes are mainly based on ideally closed systems. When considering the environments [16,17], normally the information processing which can be performed well in closed systems will be destroyed by the system-bath interaction. The detrimental effects of a Markovian [4] or non-Markovian [17–19] bath on the QST through spin chains was investigated recently. The transmission fidelity was found to decrease with the increasing system-environment coupling strength, environmental characteristic frequency, and temperature [17,19]. Many schemes have been proposed to reduce these adverse effects, like modulating the couplings between the spins [4–6] or invoking a leakage elimination operator (LEO) [17,19]. In our recent work, we investigated the almost exact state

transmission in a spin chain by adding a LEO Hamiltonian [10,17]. The LEO Hamiltonian can be realized by a sequence of control pulses. The pulse conditions have been obtained in a closed system for almost exact QST [17]. When applying these conditions to an open system, the fidelity decreases due to the existence of the environments [17,20].

Gradient descent is the most basic optimization algorithm [21], moving relevant parameters towards the direction minimizing a predefined cost, or loss, function but without guaranteeing a fast and stable convergence. The Momentum algorithm makes progress with this problem by updating parameters according to the gradients of current and previous iterations [22]. In addition, one of the algorithms with adaptive learning rates, RMSProp [23], can modulate the learning rate on the basis of different parameters and training phases. The Adaptive Moment Estimation (Adam) algorithm builds on and hence inherits the above two ones, realizing more efficient convergence behaviors, and becomes the most popular optimizer even in the noisy intermediate-scale quantum (NISQ) device era [24–26]. Recently, we used the stochastic gradient descent or Adam algorithm to find the optimized pulses for the adiabatic speedup [27] or nonadiabatic QST [28] in a noisy environment. The control pulses are designed via optimization algorithms by considering both the system and environment. As stated above, the ideal pulses are not effective for the open systems. In this paper, we use the Adam algorithm to design the optimized couplings or pulses for high-fidelity QST through a spin chain in a non-Markovian environment. By defining an effective loss function, which is relevant to the system and environmental parameters, the real unknown parameters can be revealed and the optimized solution obtained along the gradient descent direction. We adopt a newly developed non-Markovian quantum master equation approach to solve the corresponding dynamics of the system [29]. For the optimized couplings, we find that

*wangzhaoming@ouc.edu.cn

the achievable maximum fidelity can be enhanced and the corresponding arrival time can be shortened as well. For the optimized control pulses, our results show that they can acquire better QST qualities than do the ideal closed-system pulses. In both scenarios, the effects of system-bath coupling strength Γ , environmental non-Markovianity γ , and temperature T on the fidelity are analyzed. The fidelity decreases with increasing anyone of the above parameters as expected, but the fidelity can be improved by our optimized schemes, especially in a strong environment.

II. MODEL AND METHOD

When a quantum system is exposed to its environment, the total Hamiltonian H_{tot} consists of three parts

$$H_{\text{tot}} = H_s + H_b + H_{\text{int}}. \quad (1)$$

Here H_s and

$$H_b = \sum_k \omega_k b_k^\dagger b_k \quad (2)$$

are the system and bath Hamiltonian, respectively. ω_k indicates the k th mode frequency of the bath and b_k^\dagger (b_k) represents the bosonic creation (annihilation) operator, while

$$H_{\text{int}} = \sum_k (g_k^* L^\dagger b_k + g_k L b_k^\dagger) \quad (3)$$

accounts for the interaction between the system of interest and its bath. The system is linearly coupled to a bosonic bath through the Lindblad operator L with coupling constant g_k .

Assume that the bath is initially in a thermal equilibrium state at temperature T ,

$$\rho(0) = e^{-\beta H_b} / Z. \quad (4)$$

Here $Z = \text{Tr}[e^{-\beta H_b}]$ is the partition function with $\beta = 1/(K_B T)$. To deal with a finite-temperature heat bath, here we add a fictitious heat bath with the bosonic operators c_k^\dagger , c_k to the original one and guarantee that the initial state is the thermal equilibrium state in Eq. (4) after tracing over the fictitious variables. Then the total Hamiltonian with the fictitious bath is given by

$$H_{\text{tot}} = H_s + \sum_k (g_k^* L^\dagger b_k + \text{H.c.}) + \sum_k \omega_k b_k^\dagger b_k - \sum_k \omega_k c_k^\dagger c_k. \quad (5)$$

Introducing the boson Bogoliubov transformation

$$b_k = \sqrt{\bar{n}_k + 1} d_k + \sqrt{\bar{n}_k} e_k^\dagger, \quad (6)$$

$$c_k = \sqrt{\bar{n}_k + 1} e_k + \sqrt{\bar{n}_k} d_k^\dagger, \quad (7)$$

which formally couples the system to two sets of bosonic operators d_k , d_k^\dagger and e_k , e_k^\dagger . Here $\bar{n}_k = \frac{1}{\exp(\beta \hbar \omega_k) - 1}$ is the mean thermal occupation number of quanta in mode ω_k . As a consequence, the Hamiltonian in Eq. (5) becomes

$$H_{\text{tot}} = H_s + \sum_k \sqrt{\bar{n}_k + 1} (g_k^* L^\dagger d_k + \text{H.c.}) + \sum_k \omega_k d_k^\dagger d_k + \sum_k \sqrt{\bar{n}_k} (g_k^* L^\dagger e_k^\dagger + \text{H.c.}) - \sum_k \omega_k e_k^\dagger e_k. \quad (8)$$

This procedure converts the finite-temperature problem to a zero-temperature one. The initial state of the bath is $|\mathbf{0}\rangle = |\mathbf{0}\rangle_d \otimes |\mathbf{0}\rangle_e$, satisfying $d_k |\mathbf{0}\rangle_d = 0$ and $e_k |\mathbf{0}\rangle_e = 0$.

Now we introduce the quantum state diffusion (QSD) equation approach here to solve the open system dynamics [30,31]. Its major idea is to project the total wave function $|\Psi_t(t)\rangle$ to the coherent states of the bath modes $|z\rangle$ and $|w\rangle$. Then the pure state for the system $|\Psi_t(z^*, w^*)\rangle = \langle z, w | \Psi_t(t) \rangle$ becomes attainable, which is commonly known as the stochastic quantum trajectory and satisfies the following QSD equation [30]:

$$\frac{\partial |\Psi_t\rangle}{\partial t} = \left[-iH_s + Lz_t^* - L^\dagger \int ds \alpha_z(t-s) \frac{\delta}{\delta z_s^*} + L^\dagger w_t^* - L \int ds \alpha_w(t-s) \frac{\delta}{\delta w_s^*} \right] |\Psi_t\rangle. \quad (9)$$

Here

$$\alpha_z(t-s) = \sum_k (\bar{n}_k + 1) |g_k|^2 e^{-i\omega_k(t-s)}, \quad (10)$$

$$\alpha_w(t-s) = \sum_k \bar{n}_k |g_k|^2 e^{i\omega_k(t-s)} \quad (11)$$

are the bath correlation functions and

$$z_t^* = -i \sum_k \sqrt{\bar{n}_k + 1} g_k z_k^* e^{i\omega_k t}, \quad (12)$$

$$w_t^* = -i \sum_k \sqrt{\bar{n}_k} g_k^* w_k^* e^{i\omega_k t} \quad (13)$$

are the complex Gaussian noises, which meet the conditions $M[z_t z_s^*] = \alpha_z(t-s)$ and $M[w_t w_s^*] = \alpha_w(t-s)$. $M[\cdot]$ is the ensemble average over some complex Gaussian stochastic process z : $M[\mathcal{F}] = \prod_k \frac{1}{\pi} \int e^{-|z|^2} \mathcal{F} d^2 z$.

To convert Eq. (9) to a time-local form, first define the $O_{z,(w)}$ operators

$$\frac{\delta |\Psi_t\rangle}{\delta z_s^*} = O_z(t, s, z^*, w^*) |\Psi_t\rangle, \quad (14)$$

$$\frac{\delta |\Psi_t\rangle}{\delta w_s^*} = O_w(t, s, z^*, w^*) |\Psi_t\rangle, \quad (15)$$

then Eq. (9) can be written as

$$\frac{\partial |\Psi_t\rangle}{\partial t} = (-iH_s + Lz_t^* - L^\dagger \bar{O}_z + L^\dagger w_t^* - L \bar{O}_w) |\Psi_t\rangle, \quad (16)$$

where $\bar{O}_{z,(w)}(t) = \int_0^t ds \alpha_{z,(w)}(t-s) O_{z,(w)}(t, s)$. Now the determination of the $O_{z,(w)}$ operators becomes the key to solving the system dynamics in Eq. (16). However, it is usually not easy to find their explicit expressions, except for a few simple models. On the basis of Eq. (16), here we will derive an approximate non-Markovian master equation as follows.

From the consistency condition $\frac{\partial}{\partial t} \frac{\delta |\Psi_t\rangle}{\delta z_s^*} = \frac{\delta}{\delta z_s^*} \frac{\partial |\Psi_t\rangle}{\partial t}$ and $\frac{\partial}{\partial t} \frac{\delta |\Psi_t\rangle}{\delta w_s^*} = \frac{\delta}{\delta w_s^*} \frac{\partial |\Psi_t\rangle}{\partial t}$, the $O_{z,(w)}$ operators in Eqs. (14) and (15) can be determined:

$$\frac{\partial O_z}{\partial t} = [-iH_s + Lz_t^* - L^\dagger \bar{O}_z + L^\dagger w_t^* - L \bar{O}_w, O_z] - \left(L^\dagger \frac{\delta \bar{O}_z}{\delta z_s^*} + L \frac{\delta \bar{O}_w}{\delta w_s^*} \right), \quad (17)$$

$$\frac{\partial O_w}{\partial t} = [-iH_s + Lz_t^* - L^\dagger \bar{O}_z + L^\dagger w_t^* - L\bar{O}_w, O_w] - \left(L^\dagger \frac{\delta \bar{O}_z}{\delta w_s^*} + L \frac{\delta \bar{O}_w}{\delta w_s^*} \right). \quad (18)$$

Instead of a numerical simulation for the quantum trajectories, we analytically take the ensemble average to obtain a non-Markovian master equation. Define $P_t = |\Psi_t\rangle\langle\Psi_t|$, then $\rho_s = M[P_t]$. Taking the Novikov's theorem [32], Eq. (16) can be rewritten as

$$\frac{\partial}{\partial t} \rho_s = -i[H_s, \rho_s] + [L, M[P_t \bar{O}_z^\dagger]] - [L^\dagger, M[\bar{O}_z P_t]] + [L^\dagger, M[P_t \bar{O}_w^\dagger]] - [L, M[\bar{O}_w P_t]], \quad (19)$$

which is the general master equation for the system, but still not closed. Normally, the $\bar{O}_{z,(w)}$ operators contain noise except for some special cases. For instance, when the system Hamiltonian H_s commutes with the Lindblad operator, $\bar{O}_{z,(w)}$ proves to be noise-independent. When the coupling of the bath to the system is weak, the originally noise-dependent operators $\bar{O}_{z,(w)}(t, z^*, w^*)$ can be approximated well [33] by the noise-independent ones $\bar{O}_{z,(w)}(t)$. That leads us to a closed master equation

$$\frac{\partial}{\partial t} \rho_s = -i[H_s, \rho_s] + [L, \rho_s \bar{O}_z^\dagger(t)] - [L^\dagger, \bar{O}_z(t) \rho_s] + [L^\dagger, \rho_s \bar{O}_w^\dagger(t)] - [L, \bar{O}_w(t) \rho_s]. \quad (20)$$

Here we state that the system Hamiltonian H_s can be time-dependent or time-independent. A time-dependent Hamiltonian in this model was used to study the adiabatic speedup in an open system [34]. The spectral density $J(\omega)$ characterizes the frequency-dependent system-bath couplings. Taking the limit of a continuum of frequencies, the correlation functions in Eqs. (10) and (11) turn into

$$\alpha_z(t-s) = \int d\omega J(\omega) (\bar{n}_k + 1) e^{-i\omega(t-s)}, \quad (21)$$

$$\alpha_w(t-s) = \int d\omega J(\omega) \bar{n}_k^j e^{i\omega(t-s)}. \quad (22)$$

When the system-bath coupling is weak, and in the high-temperature or low-frequency limit, $\frac{1}{\bar{n}_k+1} \approx T/\omega$ (set $K_B = 1 = \hbar$). In this work, we consider the Ohmic type with a Lorentz-Drude cutoff function, which reads $J(\omega) = \frac{\Gamma}{\pi} \frac{\omega}{1+(\frac{\omega}{\gamma})^2}$ [35–37]. This spectrum can emerge in different systems, such as optomechanical systems [38,39], semiconductor optical plasmons [40], Fe-pnictides [41], and qubit-cavity coupling systems [42,43]. Here Γ stands for the system-bath coupling strength and γ is the characteristic frequency of bath. They both are real parameters. After these approximations,

$$\alpha_z(t-s) = \Gamma T \Lambda(t,s) + i\Gamma \Lambda(t,s), \quad (23)$$

$$\alpha_w(t-s) = \Gamma T \Lambda(t,s). \quad (24)$$

Here the Ornstein-Uhlenbeck correlation function $\Lambda(t,s) = \frac{\gamma}{2} e^{-\gamma|t-s|}$. It decays exponentially with the environmental memory time $1/\gamma$, which characterizes the memory capacity of the bath. Therefore, for small γ , non-Markovian properties can be observed. The large γ corresponds to a Markovian bath due to the shrinking environmental memory time. Furthermore, the correlation function satisfies the relation

$$\frac{\partial \alpha_{z(w)}(t-s)}{\partial t} = -\gamma \alpha_{z(w)}(t-s). \quad (25)$$

Now we finally obtain

$$\frac{\partial \bar{O}_z}{\partial t} = \left(\frac{\Gamma T \gamma}{2} - \frac{i\Gamma \gamma^2}{2} \right) L - \gamma \bar{O}_z - [iH_s + L^\dagger \bar{O}_z + L\bar{O}_w, \bar{O}_z], \quad (26)$$

$$\frac{\partial \bar{O}_w}{\partial t} = \frac{\Gamma T \gamma}{2} L^\dagger - \gamma \bar{O}_w - [iH_s + L^\dagger \bar{O}_z + L\bar{O}_w, \bar{O}_w]. \quad (27)$$

As a result, we are allowed to numerically solve the dynamical evolution equation in Eq. (20), with the help of Eqs. (26) and (27).

When $\gamma \rightarrow \infty$, the bath becomes completely Markovian and no longer has any memory capacity. Consequently, $\bar{O}_z = \frac{\Gamma T}{2} L$ and $\bar{O}_w = \frac{\Gamma T}{2} L^\dagger$. The master equation in Eq. (20) therefore reduces to the Lindblad form [29]

$$\frac{\partial}{\partial t} \rho_s = -i[H_s, \rho_s] + \frac{\Gamma T}{2} [(2L\rho_s L^\dagger - L^\dagger L\rho_s - \rho_s L^\dagger L) + (2L^\dagger \rho_s L - LL^\dagger \rho_s - \rho_s LL^\dagger)]. \quad (28)$$

In this paper, we consider a one-dimensional Heisenberg XY Hamiltonian as the system Hamiltonian [44]

$$H_s = \sum_{i=1}^{N-1} J_{i,i+1} (\sigma_i^x \sigma_{i+1}^x + \sigma_i^y \sigma_{i+1}^y). \quad (29)$$

Here σ_i^α ($\alpha = x, y$) stands for the Pauli operator acting on the i th spin. $J_{i,i+1}$ indicates the relevant coupling strength between the nearest-neighbor sites $i, i+1$ and we set the PST coupling layout $J_{i,i+1} = -\sqrt{i(N-i)}$ throughout. Equation (29) describes the interactions between the nearest-neighbor spins, which can be experimentally realized by quantum dots [14], ultracold atoms in optical lattices [13], or trapped ions [12]. This model can also be used to describe atoms in cavities [43], Josephson charge states [45], or phase qubits [46]. A collective bath can be electromagnetic environments [47]. A recent experiment also shows that the collective baths exist. Charge noises in a superconducting multiqubit circuit chip are observed as highly correlated on a length scale over 600 micrometres [48].

Initially, we prepared all the spins at the down state, but the first one at the up state, i.e., $|\Psi_s(0)\rangle = |1\rangle = |100 \cdots 0\rangle$. Our task is to transfer the state $|1\rangle$ from the first to the last spin of the chain, and the target state will be $|\mathbf{N}\rangle = |000 \cdots 1\rangle$. During this process, the transmission fidelity $F(t) = \sqrt{\langle \mathbf{N} | \rho_s(t) | \mathbf{N} \rangle}$ is monitored to evaluate the transfer quality. Here $\rho_s(t)$ is the reduced density matrix of our system.

Combining the advantages of two algorithms with fast and steady convergence, Momentum and RMSProp, Adam has already become the most valuable optimizer in the NISQ era [24–26]. Now in this work we use Adam to construct an iterative process to optimize the parameters for high-fidelity state transfer in noisy environments.

First we need to define a loss function $Loss$ and our goal of high-fidelity QST is encoded as to minimize the $Loss$. The specific optimization procedure of Adam algorithm is as follows.

Step 1: Compute the gradient vector \mathbf{g} of loss function $Loss$ with respect to selected variables \mathbf{A} (i.e., nearest-neighbor couplings or control pulses in our work) in the k th iteration

$$\mathbf{g}^k = \nabla_{\mathbf{A}^k} Loss(\mathbf{A}^k). \quad (30)$$

Step 2: Compute the new exponential moving averages

$$\mathbf{m}^k = \beta_1 \mathbf{m}^{k-1} + (1 - \beta_1) \mathbf{g}^k, \quad (31)$$

$$\mathbf{v}^k = \beta_2 \mathbf{v}^{k-1} + (1 - \beta_2) (\mathbf{g}^k)^2. \quad (32)$$

Step 3: Compute the new bias-corrected moment vectors

$$\hat{\mathbf{m}}^k = \mathbf{m}^k / [1 - (\beta_1)^k], \quad (33)$$

$$\hat{\mathbf{v}}^k = \mathbf{v}^k / [1 - (\beta_2)^k]. \quad (34)$$

Step 4: Update the variables \mathbf{A} according to

$$\mathbf{A}^{k+1} = \mathbf{A}^k - \alpha \hat{\mathbf{m}}^k / (\sqrt{\hat{\mathbf{v}}^k} + \varepsilon). \quad (35)$$

Step 5: Repeat steps 1 to 4 till $Loss < \xi$ or the number of iterations $k > k_{\max} \cdot \xi$ and k_{\max} are the prescribed loss ceiling and maximal iteration number (set $\xi = 0.001$ and $k_{\max} = 1000$ throughout), respectively.

III. RESULTS AND DISCUSSIONS

In this work, we consider two scenarios and apply the Adam optimizer to explore high-fidelity QST through a spin chain in open systems. For the first one, we choose to modulate the coupling strength sequence $\mathbf{J} = [J_{1,2}, J_{2,3}, \dots, J_{N-1,N}]$. For the second one, we optimize the pulse amplitude sequence $\mathbf{I} = [I_0, I_1, \dots, I_{M-1}]$ to realize a more effective LEO. We first take the Lindblad operator $L = \sum_{i=1}^N \sigma_i^-$ as an example. It indicates the dissipation [10,49]. Here $\sigma_i^- = (\sigma_i^x - i\sigma_i^y)/2$ denotes the lowering operator on the i th spin. Note that the rotating wave approximation (RWA) is used when $L = \sum_{i=1}^N \sigma_i^-$ along with the Hamiltonian in Eq. (3). The RWA is known to be accurate when the system-bath coupling is weak [50]. We only consider the weak coupling ($J/\Gamma \gg 1$) cases throughout, and then our choices of parameters are compatible with the RWA.

To begin with, we try different optimization algorithms (RMSProp, Momentum, and Adam) and compare the convergence behaviors of these three gradient-based algorithms. In Fig. 1 we plot the maximal fidelity F_{\max} as functions of iterations for the three algorithms. Here we take an optimized coupling case, for example, and the corresponding parameters are $N = 6$, $\Gamma = 0.1$, $\gamma = 1$, and $T = 10$. Obviously, compared to RMSProp, Adam converges at a little slower speed,

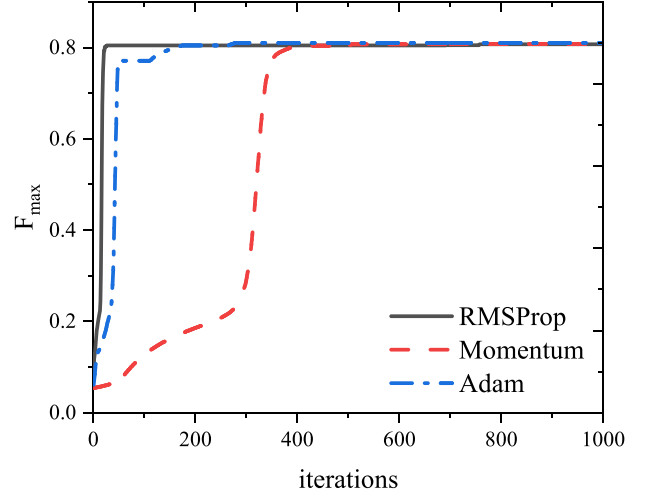


FIG. 1. Convergence behaviors of RMSProp, Momentum, and Adam algorithms. Here $N = 6$, $\Gamma = 0.1$, $\gamma = 1$, and $T = 10$.

but to a higher fidelity. As for Momentum, it has no advantage in either the speed or convergence value. From now on, we use Adam alone.

A. Optimized couplings via Adam

In this section, we perform the coupling optimization. Recall that our goal is to minimize a commonly defined loss function

$$Loss(\mathbf{J}) = 1 - F(\mathbf{J}) + \lambda J_{\max}, \quad (36)$$

where the fidelity $F(\mathbf{J})$ is obtained with the help of the optimized coupling sequence \mathbf{J} and $Loss(\mathbf{J})$ is the corresponding loss. J_{\max} stands for the maximal absolute value of couplings $J_{i,i+1}$ in optimized couplings. The relaxation parameter λ is introduced here as in Ref. [51] to modulate the proportion of J_{\max} in $Loss$ to restrain J_{\max} to not too large because it is experimentally difficult to realize a big coupling between spins.

As an example, the number of spins is taken as $N = 6$. Here we take the PST couplings $J_{i,i+1} = -\sqrt{i(N-i)}$ as an initial guess. For a fair comparison between PST and optimized couplings, the optimized ones are limited in $[-3, -2]$, which is the same region as that of the PST couplings. In addition, it is necessary to mention that, in closed systems, PST can be observed at $t = n\pi/4$ (n is an odd integer) for the PST couplings. Accordingly, the total evolution time is taken as $T_{\text{tot}} = \pi/4$ throughout. In Fig. 2 we plot the time evolution of the fidelity $F(t/T_{\text{tot}})$ with PST and optimized couplings for different environmental parameters. The parameters are taken as $\gamma = 2$, $T = 10$ [Fig. 2(a)], $\Gamma = 0.1$, $T = 10$ [Fig. 2(b)], and $\Gamma = 0.1$, $\gamma = 2$ [Fig. 2(c)], respectively. At first, without optimization, the exposure to the environment always decreases the fidelity. A larger Γ , γ or T corresponds to a lower fidelity F , i.e., a stronger system-bath interaction, a more Markovian or higher-temperature bath will destroy the system more severely, which is in accordance with the results found in Refs. [17,19]. This result still holds for the optimized coupling cases. For example, in Fig. 2(b), the maximum fidelity $F_{\max} = 0.740$ is obtained for $\gamma = 2$ and as γ grows,

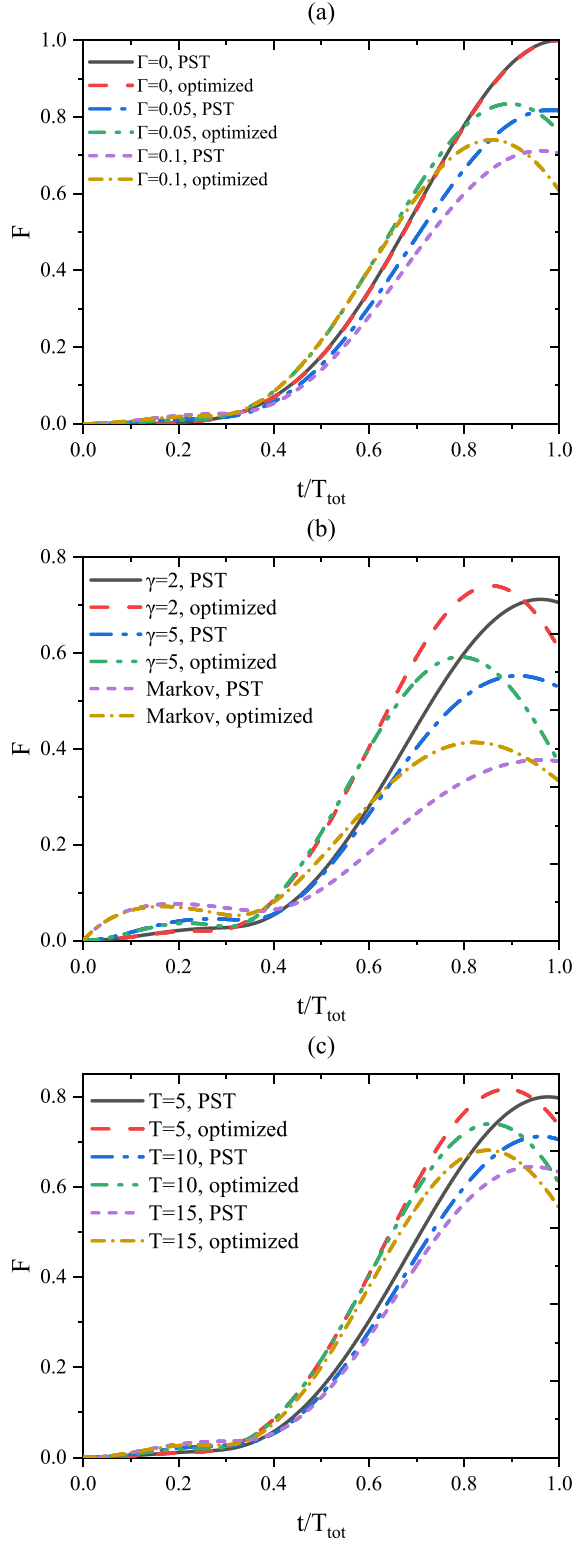


FIG. 2. The fidelity F versus the rescaled time t/T_{tot} with PST and optimized couplings for different parameters (a) Γ , $\gamma = 2$, $T = 10$; (b) γ , $\Gamma = 0.1$, $T = 10$; (c) T , $\Gamma = 0.1$, $\gamma = 2$.

F_{max} decreases. Second, comparing F_{max} for the PST and optimized couplings with the same environmental parameters, we find that the optimized F_{max} are always higher than these in the ideal cases. In other words, using the optimized couplings,

F_{max} can always be enhanced in the presence of environment. This is the key observation of our paper. It is not so obvious but worth mentioning that the maximal fidelity improvement increases with increasing Γ and T . That is to say, the bath destroys the system more severely, the improvement is more significant. Namely, a stronger bath provides more space for Adam to optimize. Clearly, without environment [$\Gamma = 0$ in Fig. 2(a)], the evolutions are same for PST and optimized couplings. Third, defining the arrival time T_a when F_{max} is achieved, with PST couplings, T_a occurs at T_{tot} for different Γ and T , and nearly at T_{tot} for different γ . The bath slightly affects the arrival time T_a for PST couplings. However, after optimization, T_a is evidently shorter than T_{tot} , which bears the advantage that F_{max} arrives earlier and thus the accumulative detrimental effects of the environment can be partially avoided. In Fig. 2, T_a is shorter for larger Γ , γ , and T . At last, even for the Markovian case [Fig. 2(b)], F_{max} can still be enhanced by the coupling optimization. In sum, our optimized couplings via the Adam algorithm can simultaneously enhance the transmission fidelity and shorten the arrival time. Figure 3 plots the corresponding PST and optimized couplings used in Fig. 2. The optimized coupling configuration is similar to the PST one: bigger in the middle and smaller in both ends. However, for a stronger bath (bigger Γ , γ , and T), Adam finds a flatter configuration, i.e., the minimum and maximum get closer. Also, the symmetry of the couplings with respect to the middle of the chain is broken due to the existence of the environments, which can be clearly seen for a strong bath [$\Gamma = 0.1$ in Fig. 3(a), $\gamma = 5$ in Fig. 3(b), or $T = 15$ in Fig. 3(c)].

B. Optimized pulses via Adam

1. QST under ideal pulse control

Environmental noise normally destroys the transmission fidelity and the authors of Refs. [19,29] introduced a LEO approach to address this problem. The main idea of this LEO approach is to add an additional Hamiltonian H_{LEO} to the system Hamiltonian H_s , ensuring the quantum system evolves along a predefined passage. For example, denoting H_{PST} as the Hamiltonian in Eq. (29) with PST couplings, we can set $|\Psi(t)\rangle = \exp(-iH_{\text{PST}}t)|\mathbf{1}\rangle$ as the evolution passage. The LEO Hamiltonian in the adiabatic frame [52] can be constructed as

$$H_{\text{LEO}} = c(t)|\Psi(t)\rangle\langle\Psi(t)|, \quad (37)$$

where $c(t)$ is the control function. The total Hamiltonian becomes

$$H_{\text{tot}} = H_s + H_{\text{LEO}}. \quad (38)$$

The LEO Hamiltonian can be achieved by a series of control pulses that can be divided into perturbative and nonperturbative versions. In this paper we consider the later one whose pulse intensity and duration are finite. The pulse conditions for effective control were theoretically deduced by the P - Q partitioning technique in closed systems [20,53,54]. For sine pulses $c(t) = I \sin(\omega t)$, the corresponding pulse condition is

$$J_0\left(\frac{I\tau}{\pi}\right) = 0. \quad (39)$$

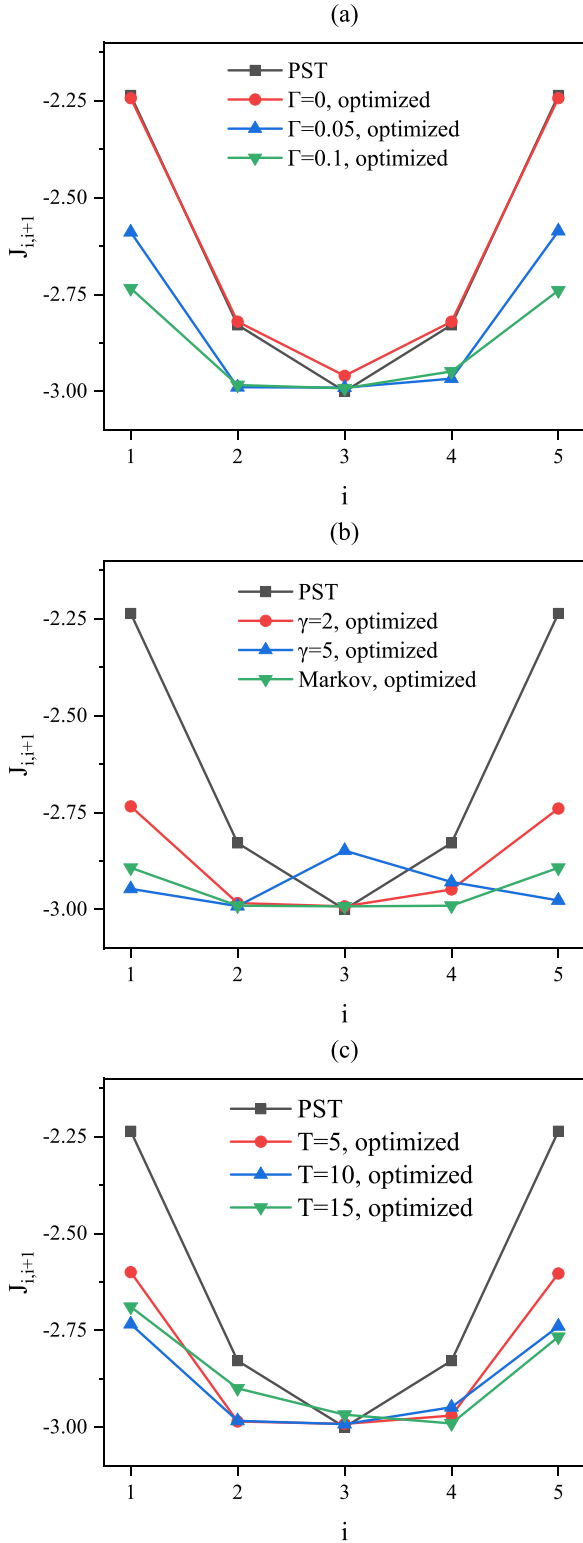


FIG. 3. The corresponding PST and optimized couplings in Fig. 2.

Here I and τ represent the pulse intensity and half period, and $J_0(x)$ denotes the zero-order Bessel function of the first kind. Note that the integral of such pulses over a period is zero (i.e., zero-area condition of pulses) [20,52]. The control pulses such as rectangular and triangular ones have also been investigated [54].

2. High-fidelity QST

Although the above ideal pulse conditions are derived theoretically from closed systems, they can be applied to open ones with no guarantee of their effectiveness. In this section, we aim to design optimized pulses for certain environmental parameters with the help of Adam, and then compare their performances with those of ideal counterparts. To make fair comparisons, the optimized pulses also satisfy the zero-area condition [20,52]. First we design the optimized sine pulses (single pulses)

$$c(t) = I(t) \sin(\omega t). \tag{40}$$

Here $I(t)$ is a P segment piecewise constant function whose P values are drawn in order from the pulse amplitude sequence $\mathbf{I} = [I_0, I_1, \dots, I_{P-1}]$ and take the equal time interval $\Delta t = T_{\text{tot}}/P$ ($\omega = 2\pi/\Delta t$ and set $P = 5$). Notice that the zero-area condition [20,52] is followed in iterative procedures as in theoretical derivation. We consider the corresponding ideal values $\mathbf{I} = [96.200, 96.200, \dots, 96.200]$, derived from the pulse condition in Eq. (39) as our initial guess. The number of spins is $N = 4$. Furthermore, the maximal intensity of the optimized pulses is not supposed to outweigh that of their ideal counterparts. Similar to Eq. (36), the loss function is accordingly defined as

$$Loss(\mathbf{I}) = 1 - F(\mathbf{I}) + \lambda c_{\text{max}}. \tag{41}$$

Here c_{max} is the maximum of the control function $c(t)$. In Eq. (41), there also is a competition between infidelity $1 - F(\mathbf{I})$ and maximal control intensity c_{max} for $Loss$, and a relaxation parameter λ to restrict c_{max} [51]. As in the previous case, it is also difficult to realize a big pulse strength experimentally. In Fig. 4, we plot the fidelity F as a function of the rescaled time t/T_{tot} for different environmental parameters with ideal and optimized pulses. In Fig. 4(a), $\gamma = 10$ and $T = 10$. When $\Gamma = 0.1$, the maximal fidelity $F_{\text{max}}(t)$ dramatically rockets, from 0.585 without control to 0.958 with ideal pulses and 0.959 with single pulses. Note that the single pulses ultimately reach the similar fidelities as the ideal pulses can do. We then propose the combinatorial sine pulses (combinatorial pulses) to obtain a higher fidelity

$$c(t) = \sum_{i=0}^{Q-1} I_i \sin [(i + 1)\omega t], \tag{42}$$

where we turn to set the control function $c(t)$ as a combination of Fourier sine components. Here Q denotes the number of Fourier components and we consider $Q = 10$. Notice that the zero-area condition [20,52] is still satisfied. Obviously, when $\Gamma = 0.1$ and 0.2, combinatorial pulses overshadow the ideal and single counterparts, and there are minor but evident increases on QST fidelities. In what follows, we choose to optimize combinatorial pulses alone. In Figs. 4(b) and 4(c), we plot the influences of the parameter γ and temperature T on the fidelity. In Fig. 4(b), $\Gamma = 0.1$ and $T = 10$ while in Fig. 4(c), $\Gamma = 0.1$ and $\gamma = 10$. For all the situations, without exception, the combinatorial pulses outshine the ideal ones. Furthermore, an increasing Γ , γ , or T corresponds to a decreasing fidelity F . Still, in a stronger bath, the optimized pulses can make larger corrections for this fidelity deteri-

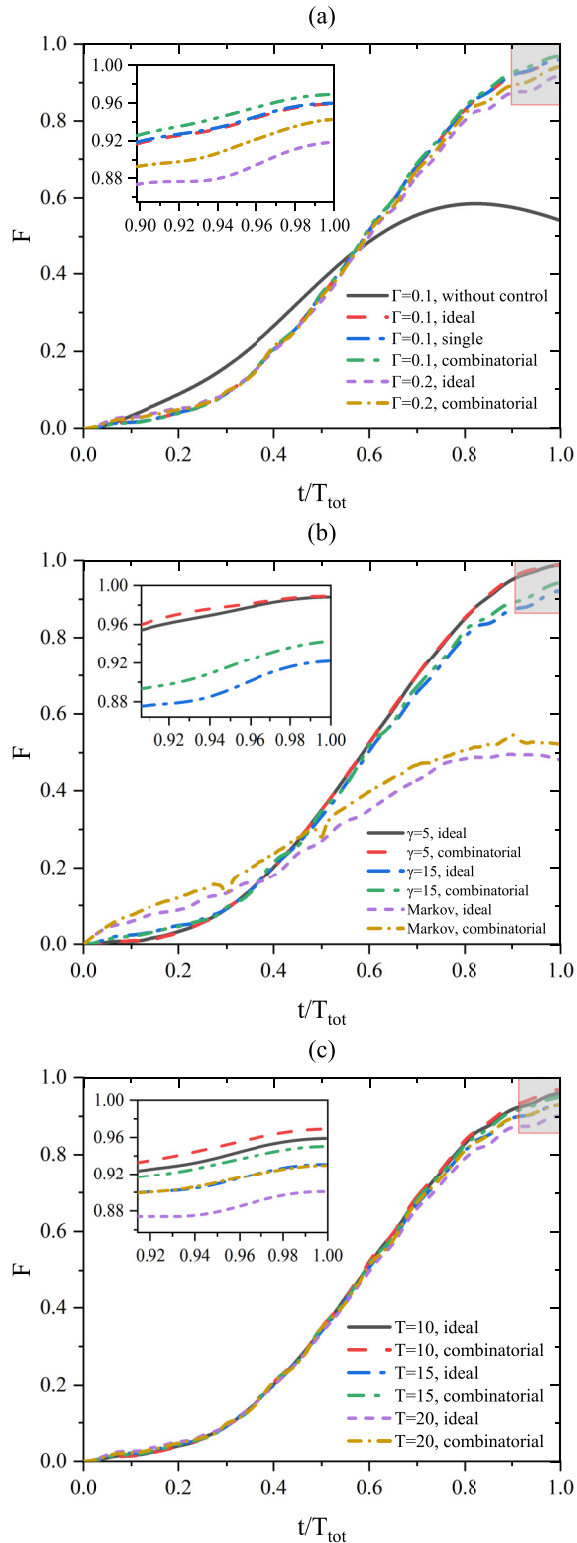


FIG. 4. The fidelity F versus the rescaled time t/T_{tot} with ideal and optimized (single and combinatorial) pulses for different parameters (a) $\Gamma, \gamma = 10, T = 10$; (b) $\gamma, \Gamma = 0.1, T = 10$; (c) $T, \Gamma = 0.1, \gamma = 10$.

oration. Figure 5 gives the profiles of corresponding ideal and optimized (single and combinatorial) pulses in Fig. 4. Figure 5(a) shows that the single pulses are almost indistinguishable from the ideal ones. As for the combinatorial

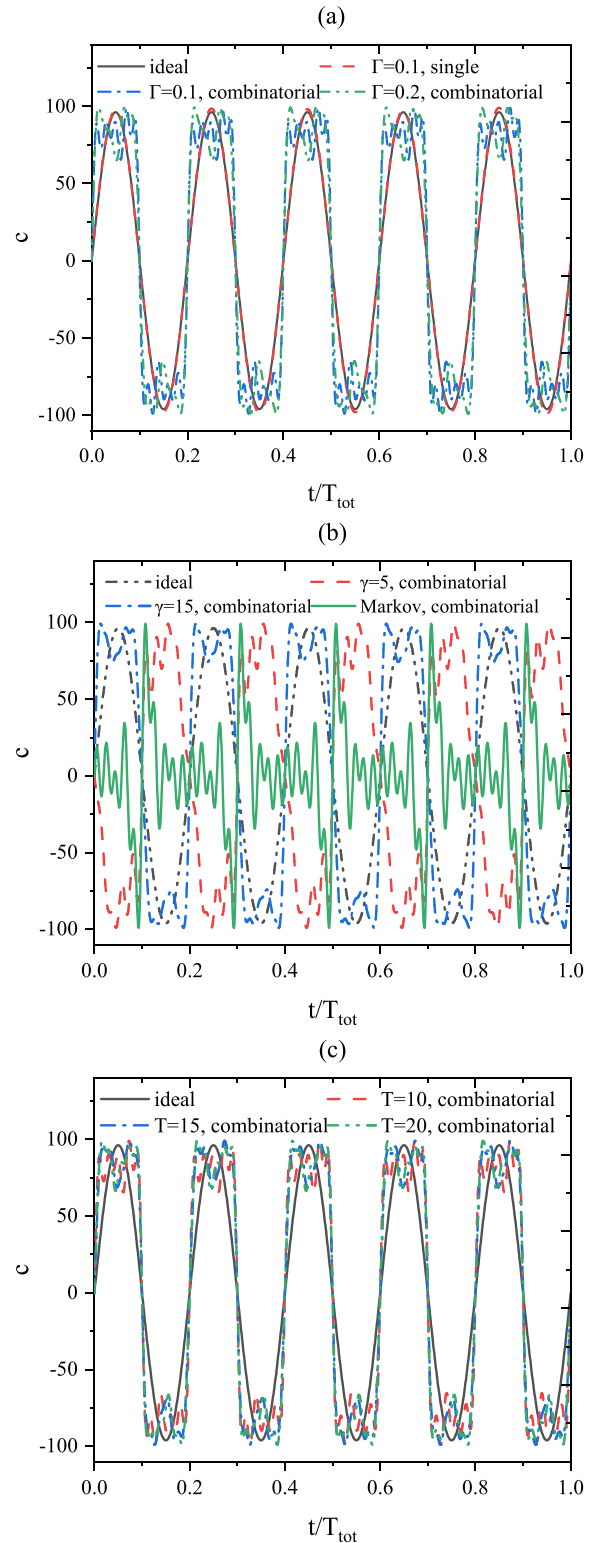


FIG. 5. The corresponding ideal and optimized (single and combinatorial) pulses in Fig. 4.

pulses, they are only similar with the ideal pulses in terms of the magnitude. From the above analysis, we conclude that the scheme of optimized control pulses can play more helpful roles than the ideal ones, especially in stronger baths.

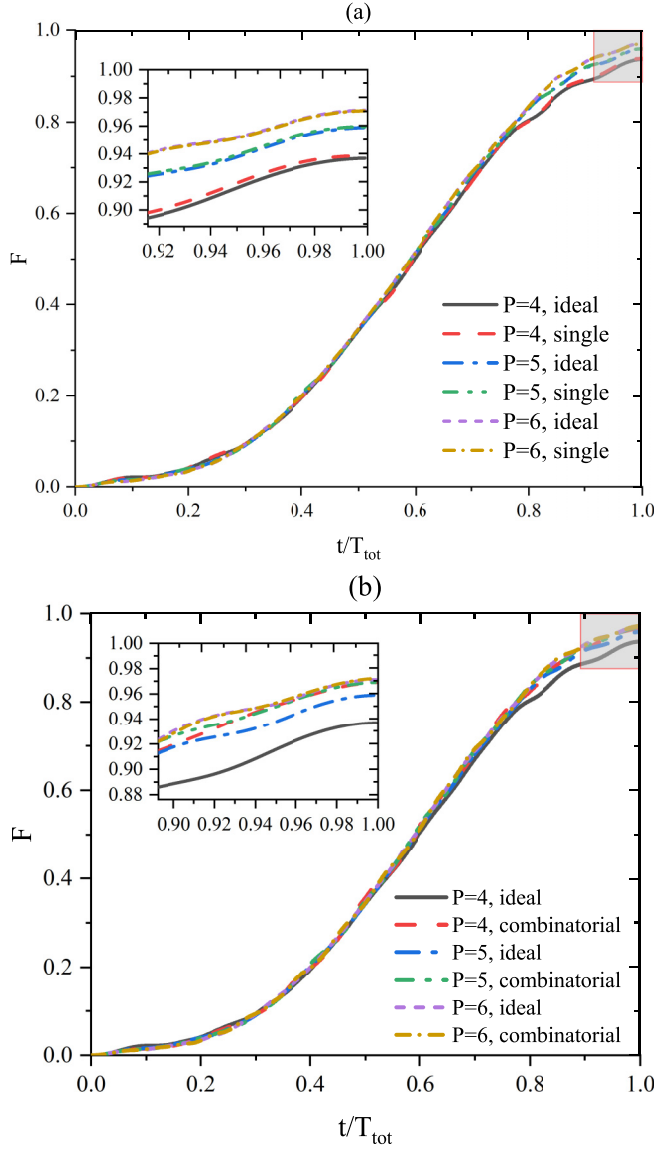


FIG. 6. The fidelity F versus the rescaled time t/T_{tot} , for different segments of the piecewise constant function $I(t)$, with (a) the ideal and single pulses; (b) the ideal and combinatorial pulses. Here $\Gamma = 0.1$, $\gamma = 10$, and $T = 10$.

Next we investigate how the segment P of the piecewise constant function $I(t)$ in Eq. (40) affects the behaviors of optimized (single and combinatorial) pulses. In Fig. 6, we plot the fidelity F versus the rescaled time t/T_{tot} for $P = 4, 5, 6$ with the ideal, single, and combinatorial pulses, respectively. The environmental parameters are still $\Gamma = 0.1$, $\gamma = 10$, and $T = 10$. Obviously, in Fig. 6(a), larger P indeed corresponds to a higher transmission fidelity, but does not lead the single pulses to a better performance than do the ideal ones. These two types of pulses still have similar results. However, Fig. 6(b) shows that, for smaller P , the combinatorial pulses are able to make more progress than the ideal ones. However, the cases with more segments have better transmission fidelities. At last we consider different types of Lindblad operator L . We will compare the effects of $L = \sum_{i=1}^N \sigma_i^-$ and

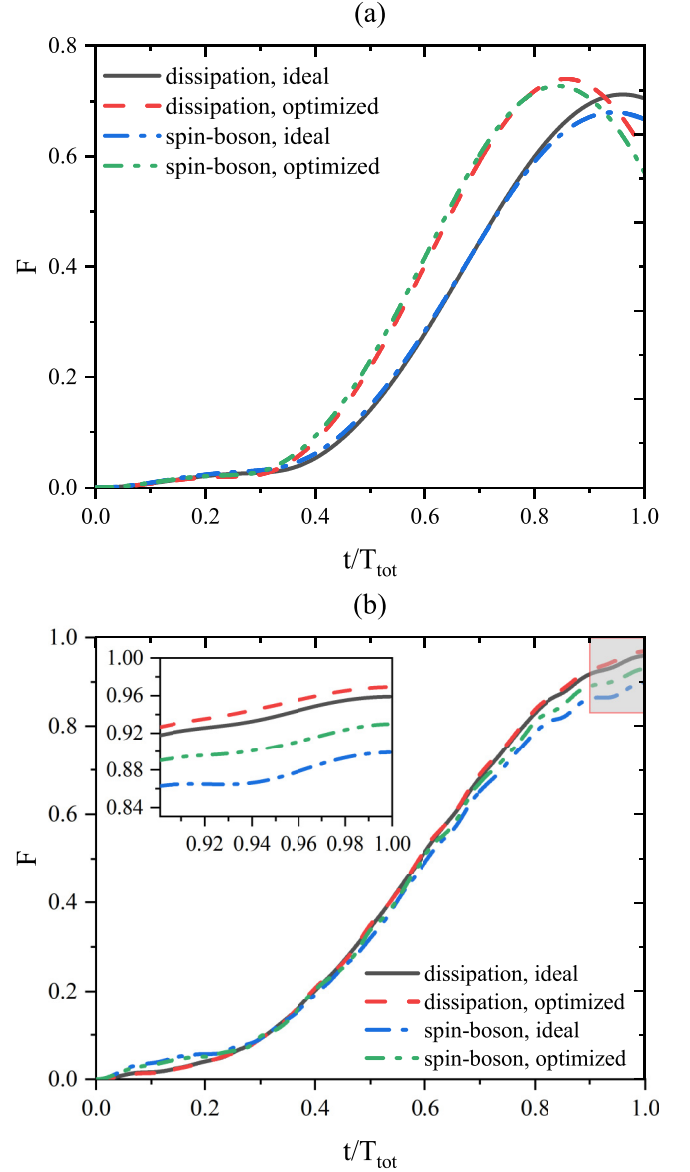


FIG. 7. The fidelity F versus the rescaled time t/T_{tot} for different Lindblad operators $L = \sum_{i=1}^N \sigma_i^x$ and $L = \sum_{i=1}^N \sigma_i^-$ with (a) PST and optimized couplings; (b) ideal and optimized (combinatorial) pulses. $T = 10$, $N = 6$, $\Gamma = 0.05$, and $\gamma = 2$ in Fig. 7(a). $N = 4$, $\Gamma = 0.1$, and $\gamma = 10$ in Fig. 7(b).

$L = \sum_{i=1}^N \sigma_i^x$ [10], and the last of these corresponds to the spin-boson interaction. We do not consider the dephasing ($L = \sum_{i=1}^N \sigma_i^z$) because $[L, \rho_s \bar{O}^\dagger] = [L^\dagger, \bar{O} \rho_s] = 0$. Therefore, the bath only randomly changes the global phase of the system [10,49,55]. In Fig. 7 we plot the cases with different Lindblad operators. Figure 7(a) shows that the fidelity obtained by the optimized couplings exceeds the PST ones regardless of what the Lindblad operator L is. The parameters are taken as $N = 6$, $\Gamma = 0.05$, $\gamma = 2$, and $T = 10$. Figure 7(b) demonstrates the implications of L on performances of optimized pulses. Again, optimized pulses show their advantages over the ideal counterparts on reducing the effects of environmental noise. We take $N = 4$, $\Gamma = 0.1$, $\gamma = 10$, and $T = 10$ in the simulations.

IV. CONCLUSION

QST is one of the basic tasks in quantum computation. PST and almost exact QST through a spin chain can be realized for PST couplings and LEO control, respectively. However, these conditions are derived theoretically from the ideally closed systems and thus their effectiveness is lost when they are applied to an open system, i.e., being coupled to a heat bath results in their dissipation dynamics. In this paper, we take a one-dimensional XY spin chain with nearest-neighbor couplings as an example and introduce a well-developed optimization algorithm, Adam, to seek for the optimized couplings and control pulses in the presence of environment. By minimizing a predefined loss function, high-fidelity transmission is obtained for both schemes. In addition, we discuss the effects of system-bath coupling strength Γ , environmental

non-Markovianity parameter γ , and temperature T on our schemes. Although the fidelity F decreases with anyone of these parameters' increasing, our optimized schemes perform better, especially for a stronger bath. Our work shows that the Adam algorithm is a powerful tool to search the optimized parameters in open quantum systems, which are important in performing quantum information processing tasks.

ACKNOWLEDGMENTS

This paper is based upon work supported by the Natural Science Foundation of Shandong Province (Grant No. ZR2021LLZ004) and Fundamental Research Funds for the Central Universities (Grant No. 202364008).

-
- [1] H. J. Kimble, The quantum internet, *Nature (London)* **453**, 1023 (2008).
- [2] T. Ramos, B. Vermersch, P. Hauke, H. Pichler, and P. Zoller, Non-Markovian dynamics in chiral quantum networks with spins and photons, *Phys. Rev. A* **93**, 062104 (2016).
- [3] S. Bose, Quantum Communication through an Unmodulated Spin Chain, *Phys. Rev. Lett.* **91**, 207901 (2003).
- [4] M.-L. Hu and H.-L. Lian, State transfer in intrinsic decoherence spin channels, *Eur. Phys. J. D* **55**, 711 (2009).
- [5] M. Christandl, N. Datta, A. Ekert, and A. J. Landahl, Perfect State Transfer in Quantum Spin Networks, *Phys. Rev. Lett.* **92**, 187902 (2004).
- [6] M. Christandl, N. Datta, T. C. Dorlas, A. Ekert, A. Kay, and A. J. Landahl, Perfect transfer of arbitrary states in quantum spin networks, *Phys. Rev. A* **71**, 032312 (2005).
- [7] J. Fitzsimons and J. Twamley, Globally Controlled Quantum Wires for Perfect Qubit Transport, Mirroring, and Computing, *Phys. Rev. Lett.* **97**, 090502 (2006).
- [8] V. Balachandran and J. Gong, Adiabatic quantum transport in a spin chain with a moving potential, *Phys. Rev. A* **77**, 012303 (2008).
- [9] M. Murphy, S. Montangero, V. Giovannetti, and T. Calarco, Communication at the quantum speed limit along a spin chain, *Phys. Rev. A* **82**, 022318 (2010).
- [10] Z.-M. Wang, F.-H. Ren, D.-W. Luo, Z.-Y. Yan, and L.-A. Wu, Almost-exact state transfer by leakage-elimination-operator control in a non-Markovian environment, *Phys. Rev. A* **102**, 042406 (2020).
- [11] X. Li, Y. Ma, J. Han, T. Chen, Y. Xu, W. Cai, H. Wang, Y. P. Song, Z.-Y. Xue, Z.-Q. Yin, and L. Sun, Perfect Quantum State Transfer in a Superconducting Qubit Chain with Parametrically Tunable Couplings, *Phys. Rev. Appl.* **10**, 054009 (2018).
- [12] J. Zeiher, J.-Y. Choi, A. Rubio-Abadal, T. Pohl, R. van Bijnen, I. Bloch, and C. Gross, Coherent Many-Body Spin Dynamics in a Long-Range Interacting Ising Chain, *Phys. Rev. X* **7**, 041063 (2017).
- [13] F. Grusdt, T. Li, I. Bloch, and E. Demler, Tunable spin-orbit coupling for ultracold atoms in two-dimensional optical lattices, *Phys. Rev. A* **95**, 063617 (2017).
- [14] M. Veldhorst, C. Yang, J. Hwang, W. Huang, J. Dehollain, J. Muhonen, S. Simmons, A. Laucht, F. Hudson, K. M. Itoh *et al.*, A two-qubit logic gate in silicon, *Nature (London)* **526**, 410 (2015).
- [15] Y. P. Kandel, H. Qiao, S. Fallahi, G. C. Gardner, M. J. Manfra, and J. M. Nichol, Adiabatic quantum state transfer in a semiconductor quantum-dot spin chain, *Nat. Commun.* **12**, 2156 (2021).
- [16] A. Ablimit, R.-H. He, Y.-Y. Xie, L.-A. Wu, and Z.-M. Wang, Quantum energy current induced coherence in a spin chain under non-Markovian environments, *Entropy* **24**, 1406 (2022).
- [17] Z.-M. Wang, M. S. Sarandy, and L.-A. Wu, Almost exact state transfer in a spin chain via pulse control, *Phys. Rev. A* **102**, 022601 (2020).
- [18] J. Jeske, N. Vogt, and J. H. Cole, Excitation and state transfer through spin chains in the presence of spatially correlated noise, *Phys. Rev. A* **88**, 062333 (2013).
- [19] S.-S. Nie, F.-H. Ren, R.-H. He, J. Wu, and Z.-M. Wang, Control cost and quantum speed limit time in controlled almost-exact state transmission in open systems, *Phys. Rev. A* **104**, 052424 (2021).
- [20] R.-H. He, R. Wang, F.-H. Ren, L.-C. Zhang, and Z.-M. Wang, Adiabatic speedup in cutting a spin chain via zero-area pulse control, *Phys. Rev. A* **103**, 052606 (2021).
- [21] X.-M. Zhang, Z. Wei, R. Asad, X.-C. Yang, and X. Wang, When does reinforcement learning stand out in quantum control? A comparative study on state preparation, *npj Quantum Inf.* **5**, 85 (2019).
- [22] I. Sutskever, J. Martens, G. Dahl, and G. Hinton, On the importance of initialization and momentum in deep learning, in *International Conference on Machine Learning* (PMLR, 2013), pp. 1139–1147.
- [23] T. Kurbiel and S. Khaleghian, Training of deep neural networks based on distance measures using RMSProp, [arXiv:1708.01911](https://arxiv.org/abs/1708.01911).
- [24] D. P. Kingma and J. Ba, Adam: A method for stochastic optimization, [arXiv:1412.6980](https://arxiv.org/abs/1412.6980).
- [25] S. J. Reddi, S. Kale, and S. Kumar, On the convergence of adam and beyond, [arXiv:1904.09237](https://arxiv.org/abs/1904.09237).
- [26] R.-H. He, X.-S. Xu, M. S. Byrd, and Z.-M. Wang, Modularized and scalable compilation for double quantum dot quantum computing, [arXiv:2211.05300](https://arxiv.org/abs/2211.05300).
- [27] Y.-Y. Xie, F.-H. Ren, R.-H. He, A. Ablimit, and Z.-M. Wang, Stochastic learning control of adiabatic speedup in a non-

- Markovian open qutrit system, *Phys. Rev. A* **106**, 062612 (2022).
- [28] X.-H. Liang, L.-A. Wu, and Z.-M. Wang, Optimally controlled non-Adiabatic quantum state transmission in the presence of quantum noise, *Photonics*, **10**, 274 (2023).
- [29] Z.-M. Wang, F.-H. Ren, D.-W. Luo, Z.-Y. Yan, and L.-A. Wu, Quantum state transmission through a spin chain in finite-temperature heat baths, *J. Phys. A: Math. Theor.* **54**, 155303 (2021).
- [30] T. Yu, Non-Markovian quantum trajectories versus master equations: Finite-temperature heat bath, *Phys. Rev. A* **69**, 062107 (2004).
- [31] L. Diósi, N. Gisin, and W. T. Strunz, Non-Markovian quantum state diffusion, *Phys. Rev. A* **58**, 1699 (1998).
- [32] S. P. Novikov, The topology summer institute (Seattle, USA, 1963), *Russ. Math. Surv.* **20**, 145 (1965).
- [33] F.-H. Ren, Z.-M. Wang, and Y.-J. Gu, Quantum state transfer through a spin chain in two non-Markovian baths, *Quantum Inf. Process.* **18**, 193 (2019).
- [34] F.-H. Ren, Z.-M. Wang, and L.-A. Wu, Accelerated adiabatic quantum search algorithm via pulse control in a non-Markovian environment, *Phys. Rev. A* **102**, 062603 (2020).
- [35] H. Wang and M. Thoss, From coherent motion to localization: II. dynamics of the spin-Boson model with sub-ohmic spectral density at zero temperature, *Chem. Phys.* **370**, 78 (2010).
- [36] G. Ritschel and A. Eisfeld, Analytic representations of bath correlation functions for Ohmic and superohmic spectral densities using simple poles, *J. Chem. Phys.* **141**, 094101 (2014).
- [37] C. Meier and D. J. Tannor, Non-Markovian evolution of the density operator in the presence of strong laser fields, *J. Chem. Phys.* **111**, 3365 (1999).
- [38] M. Aspelmeyer, T. J. Kippenberg, and F. Marquardt, Cavity optomechanics, *Rev. Mod. Phys.* **86**, 1391 (2014).
- [39] A. H. Safavi-Naeini, J. Chan, J. T. Hill, S. Gröblacher, H. Miao, Y. Chen, M. Aspelmeyer, and O. Painter, Laser noise in cavity-optomechanical cooling and thermometry, *New J. Phys.* **15**, 035007 (2013).
- [40] M. Eldlio, F. Che, and M. Cada, Drude-lorentz model of semiconductor optical plasmons, in *IAENG Transactions on Engineering Technologies: Special Issue of the World Congress on Engineering and Computer Science 2012* (Springer, New York, 2014), pp. 41–49.
- [41] S. Lee, Y.-S. Seo, S. Roh, D. Song, H. Eisaki, and J. Hwang, Correlation effects obtained from optical spectra of Fe-pnictides using an extended Drude-Lorentz model analysis, *Curr. Appl. Phys.* **39**, 90 (2022).
- [42] J. Ma, Z. Sun, X. Wang, and F. Nori, Entanglement dynamics of two qubits in a common bath, *Phys. Rev. A* **85**, 062323 (2012).
- [43] K. Luoma, W. T. Strunz, and J. Piilo, Diffusive Limit of Non-Markovian Quantum Jumps, *Phys. Rev. Lett.* **125**, 150403 (2020).
- [44] G. Mouloudakis, T. Ilias, and P. Lambropoulos, Arbitrary-length xx spin chains boundary-driven by non-Markovian environments, *Phys. Rev. A* **105**, 012429 (2022).
- [45] I. V. Pechenezhskiy, R. A. Mencia, L. B. Nguyen, Y.-H. Lin, and V. E. Manucharyan, The superconducting quasicharge qubit, *Nature (London)* **585**, 368 (2020).
- [46] J. M. Martinis, Superconducting phase qubits, *Quantum Inf. Process.* **8**, 81 (2009).
- [47] E. Ferraro, M. Scala, R. Migliore, and A. Napoli, Non-Markovian dissipative dynamics of two coupled qubits in independent reservoirs: Comparison between exact solutions and master-equation approaches, *Phys. Rev. A* **80**, 042112 (2009).
- [48] C. D. Wilen, S. Abdullah, N. Kurinsky, C. Stanford, L. Cardani, G. d’Imperio, C. Tomei, L. Faoro, L. Ioffe, C. Liu *et al.*, Correlated charge noise and relaxation errors in superconducting qubits, *Nature (London)* **594**, 369 (2021).
- [49] G. Clos and H.-P. Breuer, Quantification of memory effects in the spin-Boson model, *Phys. Rev. A* **86**, 012115 (2012).
- [50] Z.-Z. Li, C.-T. Yip, H.-Y. Deng, M. Chen, T. Yu, J. Q. You, and C.-H. Lam, Approach to solving spin-Boson dynamics via non-Markovian quantum trajectories, *Phys. Rev. A* **90**, 022122 (2014).
- [51] X.-M. Zhang, Z.-W. Cui, X. Wang, and M.-H. Yung, Automatic spin-chain learning to explore the quantum speed limit, *Phys. Rev. A* **97**, 052333 (2018).
- [52] Z.-M. Wang, M. S. Byrd, J. Jing, and L.-A. Wu, Adiabatic leakage elimination operator in an experimental framework, *Phys. Rev. A* **97**, 062312 (2018).
- [53] Y. Chen, L. Zhang, Y. Gu, and Z.-M. Wang, Acceleration of adiabatic quantum state transfer in a spin chain under zero-energy-change pulse control, *Phys. Lett. A* **382**, 2795 (2018).
- [54] L.-C. Zhang, F.-H. Ren, Y.-F. Chen, R.-H. He, Y.-J. Gu, and Z.-M. Wang, Adiabatic speedup via zero-energy-change control in a spin system, *Europhys. Lett.* **125**, 10010 (2019).
- [55] J. F. Haase, A. Smirne, J. Kołodźński, R. Demkowicz-Dobrzański, and S. F. Huelga, Fundamental limits to frequency estimation: A comprehensive microscopic perspective, *New J. Phys.* **20**, 053009 (2018).